Journal of Metals, Materials and Minerals, 36(2), e2491, 2026

Impact of chromium substitution on structural and magnetic properties of MnBi-based melt-spun ribbons

Anh Kha VUONG[1,2,3,†], Triet Minh DANG[4,†], Truong Xuan NGUYEN[1,2,*], Duy Anh Vo NGUYEN[5], Hai Van PHAM[6], Nam Hoai NGUYEN[1], Nam Hong PHAM[1], Oanh Kim Thi VUONG[1], Tan Nhut Nguyen LE[4], Tuan Van DINH[7], Nam Thanh Tran NGUYEN[6], Nhan Thi TRAN[8], Trung Quoc NGUYEN[1], Lu WEI[9], and Vuong Van NGUYEN[1]

[1] *Institute of Materials Science, Vietnam Academy of Science and Technology, No.18, Hoang Quoc Viet Road, Cau Giay district, Hanoi, Vietnam*
[2] *Graduate University of Science and Technology, Vietnam Academy of Science and Technology, No. 18, Hoang Quoc Viet Road, Cau Giay District, Hanoi, Vietnam*
[3] *Faculty of Pedagogy, Hanoi Metropolitan University, No. 98, Duong Quang Ham road, Cau Giay District, Hanoi, Vietnam*
[4] *Can Tho University, 3/2 Road, Ninh Kieu District, Can Tho, Vietnam*
[5] *FPT University, Can Tho campus, Can Tho City 900000, Vietnam*
[6] *Faculty of Physics and Institute of Natural Sciences, National University of Education, No.136, Xuan Thuy Street, Cau Giay District, Hanoi,Vietnam*
[7] *Electric Power University, No.235, Hoang Quoc Viet road, Cau Giay District, Hanoi, Vietnam*
[8] *Hanoi University of Industry, No.298, Cau Dien road, Bac Tu Liem District, Hanoi, Vietnam*
[9] *Shanghai Key Lab. of D&A for Metal-Functional Materials, School of Materials Science &Engineering, Tongji University, Shanghai 201804, China*

*** Corresponding author e-mail**: truongnx@ims.vast.vn
† These authors contributed equally

Received date:
11 August 2025
Revised date:
18 September 2025
Accepted date:
17 November 2025

Keywords:
Cr-doped MnBi magnetic material;
DFT calculation;
Magnetization;
Coercivity

Abstract

MnBi-based magnetic materials and magnets are of significant interest due to their magnetism without rare earth elements and their ability to replace Nd-Fe-B in high-temperature magnet applications due to its unique feature of enhancing coercivity in the range of 100°C to 250°C, enabling their energy product $(BH)_{max}$ comparable to NdFeB magnets despite their moderate spontaneous magnetization M_{sp}. To adjust the magnetic properties of MnBi magnets, various elements have been doped to regulate magnetic interactions among the atoms, which subsequently alters M_{sp} and the magneto-crystalline anisotropy energy. In this work, we investigate the effects of chromium doping on the magnetic properties of MnBi. The investigation includes the highlights of density functional theory (DFT) calculations and the results of doping experiments to elucidate the role of Cr dopant. The DFT consideration reveals the dynamic stability of Cr-doped MnBi system, the preferential substitution of Cr for Mn leading to the complicated modifications in the local magnetic environment. The experimental results shown the incorporation of Cr atoms into MnBi lattice and refine the microstructure of the melt-spun ribbons. Currently, the best magnetic properties are due to the $Mn_{52.5}Cr_{2.5}Bi_{45}$ annealed at 300°C for 3 h with the content of the ferromagnetic phase LTP of 65.8 wt%, the saturation magnetization measured at 30 kOe M_{sat} = 54.6 emu·g^{-1}, the coercivity iH_c = 4.2 kOe but the energy product $(BH)_{max}$ is only 3.64 MGOe.

1. Introduction

Permanent magnets have played a crucial role in societal development for many years. The phenomenon of permanent magnetism is closely tied to atomic structures and interactions within crystal unit cells and the various techniques used to prepare high-performance magnets for diverse applications. Upon on the rare earths crisis at 2010 [1], the demand for high-performance, non-rare-earth containing magnetic materials has attracted research efforts of scientists. In this pursuit, the research on MnBi magnetic material discovered in the 1950s, which achieved at this time the record room-temperature energy product of $(BH)_{max}$ = 4.5 MGOe [2] is renewed. As announced in [3], at 200°C this rare-earth-free low-cost MnBi magnetic material with the saturation magnetization M_{sat} ~ 65 emu·g^{-1}, the intrinsic coercivity iH_c ~ 20 kOe, so the energy product $(BH)_{max}$ ~ 13 MGOe is expected to be competitive with NdFeB magnets that attracts great attentions of scientific community. One understands that the 4.5 MGOe was impressive at 1950s, but far from the demands of permanent magnets applied in the current modern industry. The progress has stagnated due to challenges in increasing the content of ferromagnetic phase, which is formed at

temperatures below 340°C (denoted as the Low-Temperature-Phase (LTP)). This limitation restricts the saturation magnetization Msat and consequently, the maximum energy product $(BH)_{max}$ of MnBi magnets.

The ferromagnetism of Mn-based binary alloys is being explored using first-principles calculations, as demonstrated by researchers such as J. Park [4], M. Benaissa [5] and K. Anand [6]. These studies aim to uncover intrinsic magnetic properties like spontaneous magnetic moment, magneto-crystalline anisotropy energy and Curie temperature. The MnBi magnet stands out among these materials due to its high crystal anisotropy energy and coercivity favorable temperature-driven changes. As a result, another area of investigation focuses on the impact of different dopants on the MnBi unit cell, aiming to enhance its magnetic characteristics by optimizing atomic interactions. Bi and Mn atoms alloying forms a hexagonal unit cell structure characterized by uniaxial anisotropy. This process also influences the atomic distance between Mn atoms, maintaining it around 2.83 Å or more, as noted in Ref. [7]. This alteration converts the anti-ferromagnetic state of free Mn atoms into the ferromagnetic state observed in MnBi. Two primary methods to enhance magnetic performance through doping are replacing Mn and/or Bi atoms with High-Melting-Temperature-Point (HMTP) (in comparison with melting temperature of MnBi) elements to cause a reasonable disturbance of interactionsin inside the lattice unit cells to regulate the intrinsic magnetic properties or by Low-Melting-Temperature-Point (LMTP) elements to create grain boundary phase to regulate the extrinsic magnetic properties dependent on the samples' microstructures.

Numerous investigations have been conducted to explore the doping of MnBi. In 2013 [8], substantial efforts were directed toward enhancing its magnetic properties by doping MnBi with the high saturation magnetization element Fe, by simultaneous doping two rare-earth elements, one having positive (Sm) and the other having negative (Tb) atomic quadrupole moments, by the 5d element of Hf to couple their moments with that of Mn and two non-magnetic elements (B and C) to effect on the structural stability of doped MnBi. All the mentioned dopants decreased the magnetizations, the magneto-crystalline anisotropy energy was also moderately reduced except the significant decrease caused by Fe doping and slight increase by Boron. In 2014, titanium (Ti) [9] was introduced as a partial replacement for manganese synthesized $Mn_{50-x}Ti_xBi_{50}$ alloys. Given that, the ionic radius of Ti is comparable to that of Mn, this substitution allows for minimal disruption in the Mn-Mn distance. S. Zhang *et al.* [10] also attempted to replace Bi sites with Ti doping. However, due to their thermodynamic properties, Ti atoms cannot penetrate the unit cell of MnBi, either into Mn or Bi sites, making Ti doping ineffective. In the work of Y. Yang *et al.* [11], Gallium was doped into the Bi sites to increase the Curie temperature (T_c) from 633 K to 655 K by strengthening the magnetic interaction. However, this T_c improvement came at the cost of ~ 25% decrease in magnetization. Additionally, the doping of Cobalt (Co) into the vacant sites of Bi was recommended based on the density functional theory calculations [12]. The calculated values 4.363 μ_B of the magnetic moment and 3.06 $MJ{\cdot}m^{-3}$ for the magneto-crystalline anisotropy suggest the prospect of Co in regulating magnetism in MnBi. However, this recommendation is challenging to implement, as Cobalt atoms do not readily penetrate the unit cell of MnBi. Cu and Al were also added to MnBi alloys [13]. Although the exact penetration of Cu and Al atoms remains unknown, these additions improved coercivity at the expense of decreased magnetization. Another potential dopant, Sb, is considered a promising replacement for Bi [14–17] because hexagonal MnSb is isotopically similar to MnBi, and Bi and Sb are completely miscible. Unfortunately, this potential is undermined by the low magnetization phase of $Mn(Bi_{0.85}Sb_{0.15})$ that was stably appeared during the processing of the Mn-Bi-Sb system. The replacement of Bi with rare earth elements R (Nd and Dy) has also been investigated for compositions of $MnBi_{100-x}R_x$ [18], for which. the coercivity enhancement was observed but without any improvement of magnetization. The influences of low melting temperature point elements like Bi and Sn were investigated in [19,20]. The Bi enrichment did not enhance the LTP content but helps to align the easy axes of grains inside samples annealed in a magnetic field leading to the enhancement of the saturation magnetization M_{sat} as well the remanent magnetization M_r. These enhancements are paid by decreasing coercivities since the presence of Bi on the grain boundaries weakens the magnetical isolation between grains. The Sn dopant drops magnetization but modifies the microstructures from the spherical to rod-shaped thus allows to keep the $(BH)_{max}$ at 12.9 MGOe, 8.1 MGOe for ribbon and magnet prepared thereof, respectively.

Among HMTP elements, the ionic radius of chromium (Cr) is at 0.52 Å, notably close to the ionic radius of manganese at 0.46 Å [21], this similarity implies that the introduction of Cr is likely to cause minimal disruption to the existing structure. Cr atoms have the potential to replace manganese atoms partially or occupy interstitial sites within the bismuth matrix. As a result, chromium incorporation is anticipated to influence the electron interactions within the unit cell of chromium-doped MnBi alloys while preserving the material's ferromagnetic properties. The influences of Cr dopant on the magnetic performance of MnBi were reported in the works of K. Anand *et al.* [22,23], where the ability of Cr in enhancing both magnetization and coercivity was observed that led to the best value of 5 MGOe of $(BH)_{max}$ of Cr-doped MnBi. Here, it is worthy to note that, the undoped MnBi material has the low energy product ($(BH)_{max}$ = 0.5 MGOe). The announced magnetic performance enhancement, therefore, must be shared to both the intrinsic enhancement of the mother MnBi phase and/or the impacts of the Cr doping. In the second work, the optimal alloy composition $Mn_{47}Bi_{50}Cr_3$ has been simply used for preparing ribbons that have also the modest value $(BH)_{max}$ = 5.1 MGOe when melt-spun at 20 $m{\cdot}s^{-1}$. So, the further investigation of HMTP Cr dopant is focused to make more clear its impacts on the magnetic properties of doped MnBi that urges us to investigate the Cr doping again, and in this turn, we try by both theoretically (DFT consideration) and experimentally.

To better understand the ability of Cr dopant in adjusting the magnetic performance of MnBi material, in this work, we examine the effects of doping MnBi with Cr by using the density functional theory (DFT) calculations supplemented with the experimental results. Both studies shown that the coercivity H_c of Cr-doped MnBi can be enhanced while the spontaneous magnetization M_{sp} may have both tendency of increase as well decrease. All the results of DFT and experiments are presented in details.

2. Methods

2.1 Computational details

To explore the structural and magnetic properties of MnBi and $Mn_{55-x}Cr_xBi_{45}$, we perform first-principles calculations using the Amsterdam Modeling Suite (AMS) package [24,25]. All periodic DFT optimizations are performed using the M3GNet-UP-2022 machine learning (ML) potential [24] and the Quasi-Newton optimization approach [26]. Deep learning algorithms generate the M3GNet-UP-2022 set of potentials to provide an accuracy comparable with the generalized gradient approximation (GGA) with Perdew, Burke, and Ernzerhof (PBE) exchange−correlation functional [26]. Lattice parameters and atom coordinates are optimized until the stress-energy per atom is less than 10 eV·Å^{-1} to 5 eV·Å^{-1} and the energy difference between two consecutive steps is less than 10 eV to 3 eV.

The electronic properties of the compounds are determined using a double-zeta polarization (DZP) basis set in which the core orbitals are considered frozen during the self-consistent field procedure. Spin-polarized DFT calculations are conducted within the generalized gradient approximation (GGA) [27]. We also incorporate spin-orbit coupling (SOC) effects in non-collinear computations to precisely predict the magnetic properties of these compounds.

2.2 Sample preparation

The MnBi-based alloy of $Mn_{55}Bi_{45}$ has been chosen as a mother to which Cr-dopant is doped. To prepare the Cr-doped, Mn-enriched compositions of $Mn_{55-x}Cr_xBi_{45}$, where x is 0, 2.5, 5.0, 7.5, and 10.0, the arc-melting technique has been used with the high purity substances of Mn, Bi and Cr. To avoid the change of prepared ribbons' composition from the desired one, the starting alloys were arc-melted by using the auxiliary eutectic alloy of $Cr_{94.6}Bi_{5.4}$ [28] and the intermediate alloys of MnaBib with the balanced a and b coefficients to form the final desired composition of $Mn_{55-x}Cr_xBi_{45}$. It was observed that the weight difference of samples before and after arc-melting did not exceed 1%.

These substances were weighted for the desired compositions for 20 g batches and arc-melted inside the pits of the arc-melter. The arc power has been controlled to keep the batches melted without blue steam of boiled bismuth. A five-fold melting and flipping procedures have been implemented to ensure the homogeneity of alloys. The resulting alloys were then divided into 5 g pieces, remelted in a quartz crucible of the melt-spinner inside the 0.8 atm of argon protection gas. The melting stream was sucked on the surface of rotating wheel through the 0.8 mm orifice of the crucible positioned at 2 mm above the wheel surface. For all the experiments discussed in this paper, the wheel speed was kept at 20 m·s^{-1} which was optimal for melt-spinning undoped MnBi ribbon on the used melt-spinner. The thickness of prepared ribbons was around 20 μm, the lengths were several centimeters. The phase compositions of ribbons were analyzed using X-ray diffraction (XRD) patterns obtained from a D8-Brucker X-ray diffractometer using the Cu K_α wavelength (1.5406 Å). Further refinement of the phase presence and phase transition was conducted through differential scanning calorimetry (DSC) measurements. The LTP contents γ of samples are evaluated by using the ratio α between the intensities of two strongest peaks of MnBi(101) located at 2θ = 28.14° and Bi(012) at 27.16° and the calibration formula $\gamma = 44.6 + 51.3 \log\alpha$ presented in the previous work [29]. The microstructures of the ribbons were examined using field emission scanning electron microscopy (FESEM) with a Hitachi S-4800. The magnetic properties were evaluated by analyzing the magnetic hysteresis loops measured using a Physical Property Measurement System (VersaLab) with a maximum measuring field strength of 3 Tesla. The measured samples were flakes cut from the melt-spun ribbons, their ratio between the length to width and thickness was kept more than 3, so with the measuring field oriented along the length the demagnetization effect can be ignored.

3. Results and discussions

3.1 First-principles results of $Mn_{55-x}Cr_xBi_{45}$ melt-spun ribbons

As suggested by Ref. [31], we generate a low-temperature phase (LTP) MnBi crystal in the NiAs-type hexagonal structure (Space group No. 194). This structure contains two Mn and two Bi atoms located at the high symmetry Wyckoffs' 2a and 2c sites, respectively. The optimized lattice parameters of the pure LTP-MnBi are a = b = 4.314 Å and c = 5.950 Å, which are closely to the experimental values of a = b = 4.285 Å, c = 6.113 Å [30]. We define the formation energy of the LTP-MnBi system as [24,25]:

$$\Delta E = \frac{E_{total} - n_{Mn}.E_{Mn} - n_{Bi}.E_{Bi}}{n_{Mn} + n_{Bi}}$$

where E_{total}, E_{Mn}, and E_{Bi} are total energy, the energy of a Mn and a Bi atom in their bulk systems, respectively; and the number of Mn (n_{Mn}) and Bi atoms (n_{Bi}) are of 11 and 9 in the LTP phase. The resulting formation energy of this MnBi configuration is 0.348 eV. To create the crystal structure of $Mn_{55}Bi_{45}$, we started with the LTP-Mn_8Bi_8 structure and inserted 3 Mn and 1 Bi atom into the interstitial sites, resulting in the formation of $Mn_{11}Bi_9$, which exhibits the highest Wyckoffs's symmetry order of $Mn_{55}Bi_{45}$ (see Figure 1(a)). Next, to form the $Mn_{50}Cr_5Bi_{45}$ configuration, we substituted one Mn atom with Cr atom in the $Mn_{11}Bi_9$ supercell, and periodically extended this structure to create the $Mn_{50}Cr_5Bi_{45}$ configuration before optimization. Figure 1(a) presents all possible doping sites for the $Mn_{11}Bi_9$ crystalline structure. To identify the most energetically favorable configuration of the doped $Mn_{50}Cr_5Bi_{45}$ system, we define its formation energy as:

$$\Delta E = \frac{E_{total} - n_{Mn}.E_{Mn} - n_{Bi}.E_{Bi} - n_{Cr}.E_{Cr}}{n_{Mn} + n_{Bi} + n_{Cr}}$$

where E_{Cr} is the energy of a Cr atom in its bulk phase and n_{Cr} are the number of Cr atoms in the doped systems. Table 1 illustrates the sixth configuration as the lowest formation energy and the highest Wyckoff symmetry (see Figure 1(c-d)). Taking this configuration as the optimal structure, we applied a similar method to create the $Mn_{45}Cr_{10}Bi_{45}$ sample (see Figure 1(e-f)). As shown in Table 1, the optimal configuration for $Mn_{45}Cr_{10}Bi_{45}$ is associated with the third doping configuration.

To assess the structural stability of these systems, we calculate the phonon frequencies at high symmetry points using the M3GNet-UP-2022 machine learning potential. As illustrated in Figure 2, no imaginary frequencies along the high symmetry path exist for any of the evaluated crystalline structures. This finding indicates that these optimized structures are dynamically stable and confirms that our crystal structure generation method is appropriate.

Table 1. Lattice parameters of $Mn_{55-x}Cr_xBi_{45}$, where *x* equals 0, 5, and 10.

System	a [Å]	c [Å]	c/a	V [Å^3]
$Mn_{55}Bi_{45}$	10.470	5.779	0.552	446.687
$Mn_{50}Cr_5Bi_{45}$	9.595	5.757	0.600	441.425
$Mn_{45}Cr_{10}Bi_{45}$	9.556	5.729	0.600	437.052

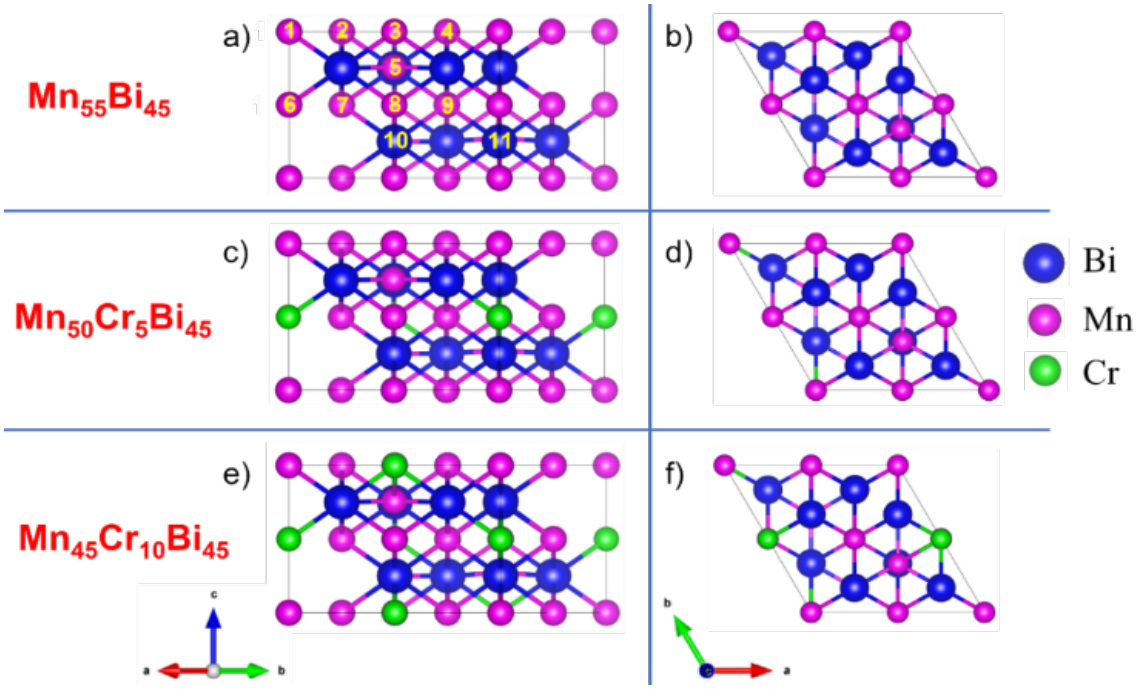

Figure 1. Side-view (left) and top-view (right) of $Mn_{55-x}Cr_xBi_{45}$, where *x* is equal to 0, 5, and 10. The blue, purple, and green balls represent Bi, Mn, and Cr atoms, respectively.

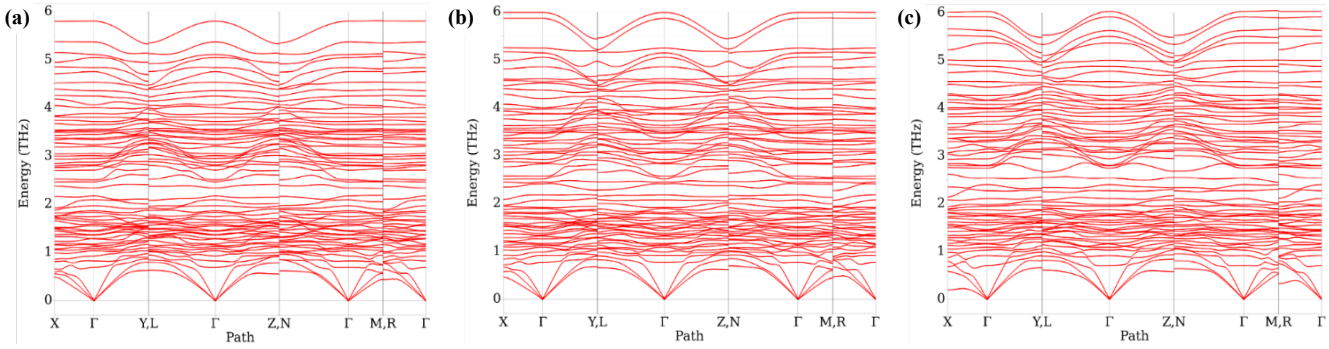

Figure 2. Phonon dispersion spectra of $Mn_{55-x}Cr_xBi_{45}$, where x equals 0 (a), 5 (b), and 10 (c).

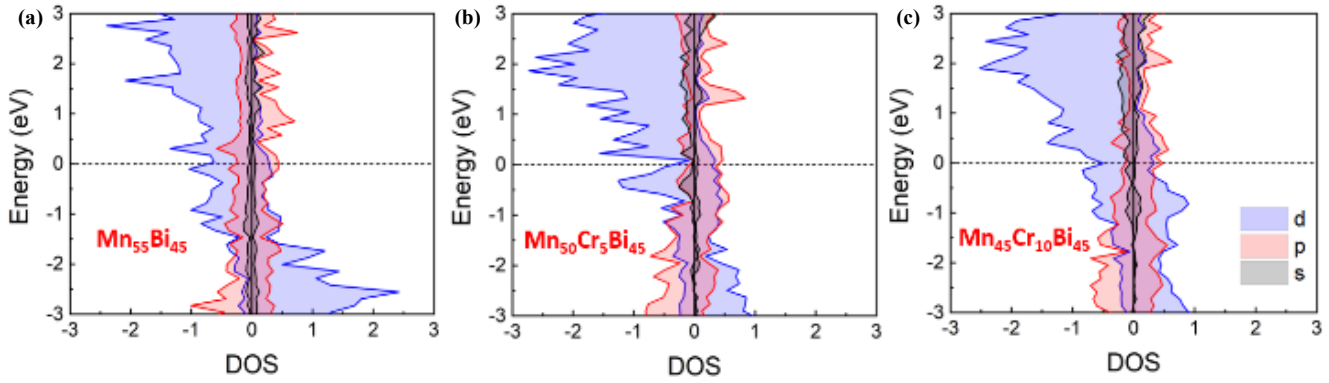

Figure 3. Projected density of states (pDOS) of $Mn_{55-x}Cr_xBi_{45}$, where *x* is equal to 0, 5, and 10.

We now evaluate the effect of doping a Cr-doped atom to the MnBi systems on their electronic and magnetic behavior. Figure 3 presents the density of states (DOS) of $Mn_{55-x}Cr_xBi_{45}$, where x is 0, 5, and 10. The Fermi level is set at zero energy to distinguish the valence and conduction states in electronic band structures, as indicated by solid black lines. In the case of $Mn_{55}Bi_{45}$ in Figure 3(a), the major electronic contribution to the DOS is from the Mn 3d-orbitals with five unpaired electrons. According to the general Pauli's principle, in ferromagnetic materials like MnBi, these neighboring spins align parallel to minimize the system's energy. Thus, the majority spin states are lower in energy than the minority spin states. In the MnBi alloy, most spin states are predominantly occupied, as the contribution to the DOS in MnBi mainly arises from the Mn 3d-orbitals. Moreover, since Mn has a half-filled 3d-orbital, the DOS contribution from the Mn atom split almost equally in both occupied and unoccupied states, with the majority state being occupied and the minority state unoccupied. The DOS around the Fermi level of $Mn_{55}Bi_{45}$ degenerates, with the majority-spin state lying just below EF, while the minority-spin state lies slightly above the Fermi level. Thus, as shown in Figure 3(a), the electronic density of states of the $Mn_{55}Bi_{45}$ system exhibits spin-splitting energy bands, as observed by the solid red and blue lines for spin-up and spin-down bands, respectively. Specifically, the spin-splitting is more evident at the low-lying energies near the Fermi level and higher conduction band. At the same time, the spin degeneration appears at the deep valence energies starting from –1.5 eV. The spin-splitting energy bands imply its ferromagnetic feature. Odd chromium atom doping increases the magnetic moment of $Mn_{50}Cr_5Bi_{45}$ by mainly contributing to the occupied states dominated by minority-spin states, leading to higher degeneracy energy states around the Fermi level. This unique contribution results in an increase in the magnetic moment of $Mn_{50}Cr_5Bi_{45}$ (Figure 3(b)). However, by doping even chromium atoms, since the contribution of minority-spin and majority-spin states is almost equal, fewer degeneracy states are observed in the density of states (Figure 3(c)). Thus, in this case, the magnetic moment slightly decreases.

Table 2 lists the calculated spin and orbital magnetic moments. In pristine $Mn_{55}Bi_{45}$ crystals, the absolute values of spin magnetic moments of Mn and Bi are recorded as 3.730 μ_B and 0.069 μ_B, along with orbital moments of 0.184 μ_B and 0.025 μ_B, which are in qualitative agreement with Ref. [32]. The polarization of Bi magnetic moment in the opposite direction of Mn can be attributed to the hybridization of Bi p-orbitals with Mn d-orbitals, leading to a reduction in the overall magnetization of the compound. In $Mn_{55-x}Cr_xBi_{45}$, the Cr doping influences the spin magnetic moment of Mn, leading to an increased spin magnetic moment with 3.869 μ_B (x=5) and 3.791 μ_B (x=10). In transition metals, the orbital magnetic moment is often suppressed due to the influence of the crystal field, leading to a relatively small orbital moment. The introduction of Cr through substitution has a pronounced effect on the overall orbital magnetic moments. A substantial portion, exceeding half of the total orbital moment, arises from the presence of Cr, contributing 0.630 μ_B (x=5) and 0.612 μ_B (x=10). Note that, due to the saturation of magnetization, a large increase of Cr atoms does not lead to significant changes in the orbital magnetic moments of Mn atoms.

To further understand the changes in magnetic moments due to Cr atom doping, we present the charge density and the planar-averaged charge density difference in Figure 4-5. The electron density map illustrates valence electronic charge density variations within the plane containing Bi atoms and vacant interstitial sites. Figure 4 shows no overlap in the charge distribution between adjacent atoms, confirming the feasibility of substituting Cr at these specific sites. Figure 5 displays the planar-averaged charge density difference along the c-direction for the $Mn_{50}Cr_5Bi_{45}$ (left) and $Mn_{45}Cr_{10}Bi_{45}$ (right) heterostructures. The yellow and cyan colors represent charge accumulation and depletion, respectively. As shown in Figure 5(a), incorporating Cr atoms, represented with arrows, emphasizes their influence on charge distribution. In the presence of Cr atoms in the $Mn_{50}Cr_5Bi_{45}$ hetero-structure, a noticeable charge redistribution occurs around Cr atoms, affecting both the electron and hole densities and enhancing charge separation, significantly increasing these materials' magnetic moments. As the number of Cr atoms in the structures increases ($Mn_{45}Cr_{10}Bi_{45}$) (see Figure 5(b)), the planar-averaged charge density difference along the c-direction suggests a more pronounced impact of Cr on the electronic structure. The Cr atoms, indicated by red arrows, contribute strongly to the local charge density changes, leading to more noticeable charge accumulation and depletion regions. This indicates that Cr doping alters the electronic properties of the alloy, slightly increasing its overall spin magnetic properties (Table 2). These density profiles also reflect how doping breaks the symmetry of the original MnBi structure, introducing localized effects near Cr atoms. These results demonstrate that Cr atoms preferentially substitute Mn within the MnBi lattice. This substitution disrupts the local magnetic environment by modifying Mn–Mn interactions, which alters the overall magnetization and coercivity. Notably, these predictions align with subsequent experimental observations, where Cr doping changes the magnetic hysteresis loops and microstructures of melt-spun ribbons.

3.2 Experimental results of $Mn_{55-x}Cr_xBi_{45}$ melt-spun ribbons

According to the phase diagram of the Mn-Bi system, the alloys MnxBiy with the compositions around the ferromagnetic phase composition $Mn_{50}Bi_{50}$ are solidified peritectically, therefore, melt-spun ribbons have a multiphase structure comprising LTP and extracted Mn and Bi phases. By annealing process these Mn and Bi are combined to form and to increase the content of LTP in final annealed ribbons. It was found that with a Mn to Bi weight ratio of 55:45, the final alloy has the highest LTP phase content [33]. Consequently, this composition has been selected as the main mother phase to study the effects of Cr dopants on the microstructure and magnetic properties of Cr-doped MnBi magnetic material in this work.

Table 2. Spin and orbital magnetic moments of $Mn_{55-x}Cr_xBi_{45}$, where *x* is equal to 0, 5 and 10.

System	Mn [μ_B]		Bi [μ_B]		Bi [μ_B]	
	Spin	Orbital	Spin	Orbital	Spin	Orbital
$Mn_{55}Bi_{45}$	3.730	0.184	0.069	0.025		
$Mn_{50}Cr_5Bi_{45}$	3.869	0.630	0.069	0.072	2.349	0.689
$Mn_{45}Cr_{10}Bi_{45}$	3.791	0.612	0.053	0.059	2.494	0.360

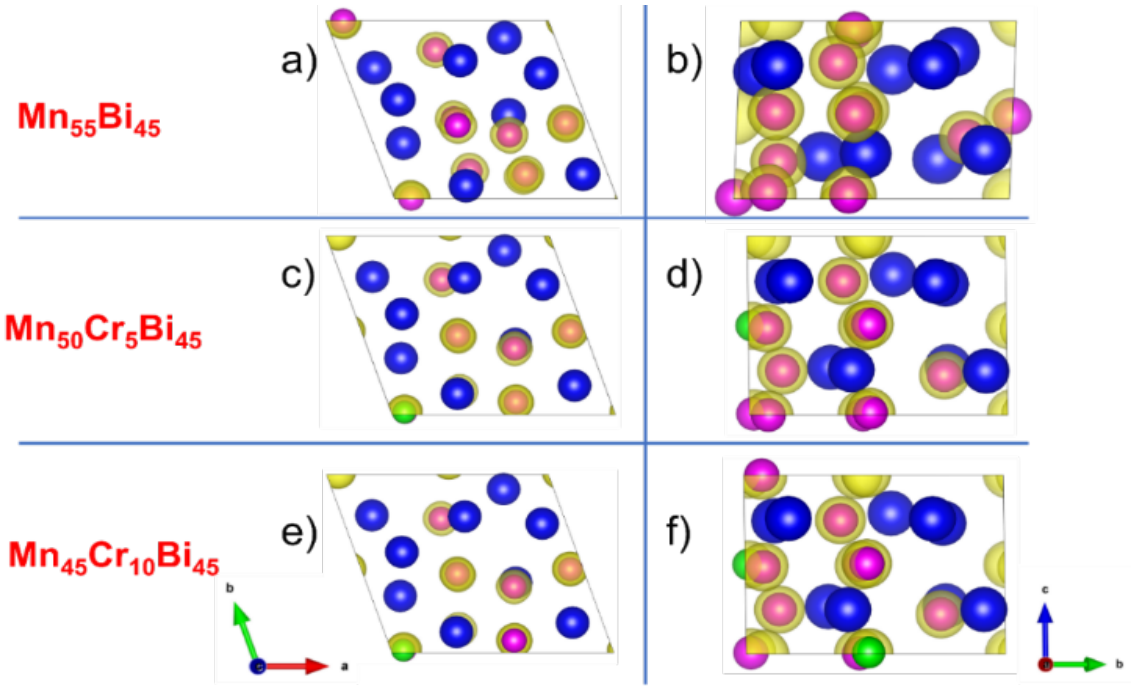

Figure 4. Top-view (left) and side-view (right) of the charge density for the $Mn_{55}Bi_{45}$ (a-b), $Mn_{50}Cr_5Bi_{45}$ (c-d), and $Mn_{45}Cr_{10}Bi_{45}$ (e-f) heterostructures, respectively. The yellow colors indicate charge accumulation and the iso-values are 0.1 e/Å^3.

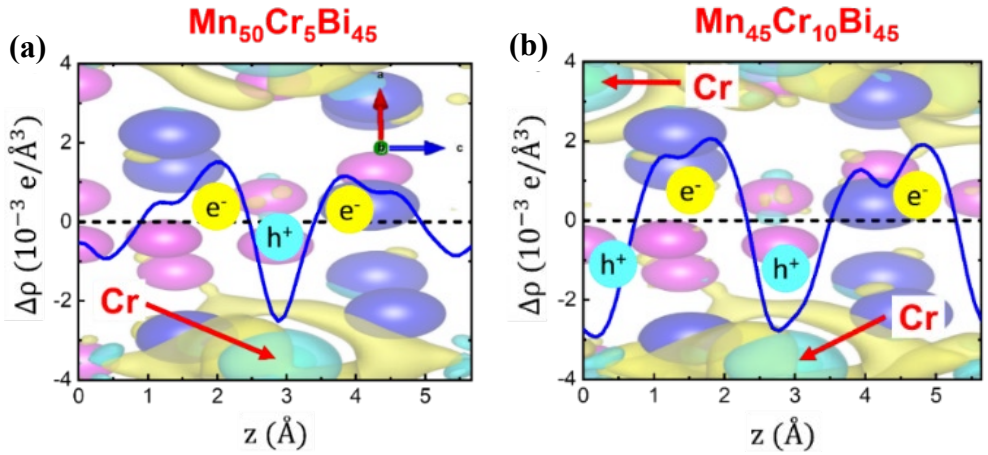

Figure 5. The planar-averaged charge density difference along the *c*-direction for the $Mn_{50}Cr_5Bi_{45}$ (left) and $Mn_{45}Cr_{10}Bi_{45}$ (right) heterostructures. The yellow and cyan colors indicate charge accumulation and depletion, respectively. The iso-values are 0.003 e/Å^3.

Figure 6 presents the XRD patterns of a series of as melt-spun ribbons $Mn_{55-x}Cr_xBi_{45}$, where x varied in the range from 0 to 10. It is understood that because of the above mentioned peritectic solidification of Mn-Bi system, the LTP contents γ of as-cast samples are low. The LTP content γ are only 28.0, 18.5, 16.8, 20.3 and 21.2 for the samples with x = 0, 2.5, 5.0, 7.5 and 10.0, respectively. A prominent feature is the disappearance of the strongest peak (110) of Cr (usually located at 46.69°) on all the patterns proposing that the doped Cr atoms have integrated into the unit cells of MnBi.

The influence of Cr dopant on the interaction between atoms inside the unit cell should affect the magnetic phase transition. The Curie temperature can be determined from DSC traces by observing an anomaly in the heat flow correlated with the change in magnetic order within the material, such as the transformation from the ferromagnetic state to the paramagnetic one as in our case. The DSC traces presented in Figure 7 for $Mn_{55-x}Cr_xBi_{45}$ melt-spun ribbons with x = 0.0 and 5.0 reveal this influence. It is observed that, the first endothermic peaks appeared at 267°C on both traces, they are due to the melting state of Bi residues in both samples, the second endothermic peaks correspond to the magnetic state transformation that show the decrease of the Curie temperature T_c from 355°C of undoped sample down to 346°C for the sample with 5 wt% of Cr dopant. The similar effect was observed in [22] where the LTP – HTP transformation has been registered.

The magnetic performance of prepared ribbons was evaluated on their magnetic hysteresis curves presented on Figure 8. The saturation magnetizations M_{sat} and coercivities H_c measured at 3 Tesla are 17.6 emu·g^{-1}, 15.2 emu·g^{-1}, 14.6 emu·g^{-1}, 13.5 emu·g^{-1}, 9.4 emu·g^{-1} and 3.3 kOe, 5.5 kOe, 4.1 kOe, 6.1 kOe, 9.2 kOe for samples with x = 0.0, 2.5, 5.0, 7.5 and 10.0 respectively, and illustrated in the graph sketched in Figure 8.

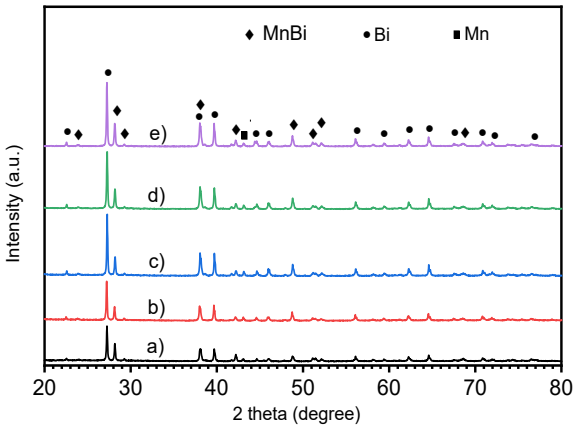

Figure 6. XRD patterns of $Mn_{55-x}Cr_xBi_{45}$ as spun ribbons: (a) x=0, (b) x = 2.5, (c) x= 5.0, (d) x = 7.5, and (e) x = 10.0.

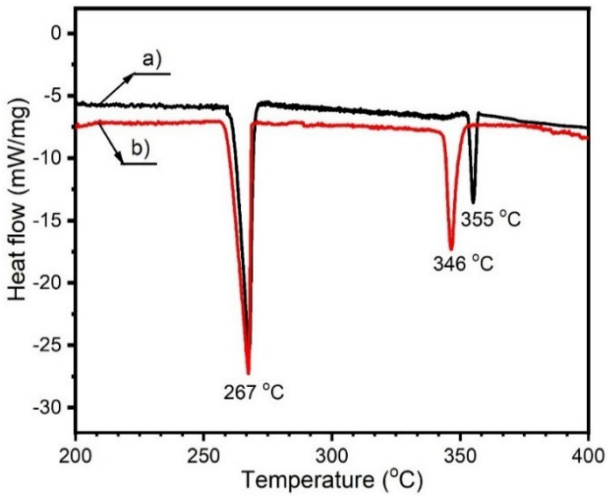

Figure 7. Differential scanning calorimetry (DSC) traces of $Mn_{55-x}Cr_xBi_{45}$ melt-spun ribbons: (a) x=0, and (b) x = 5.

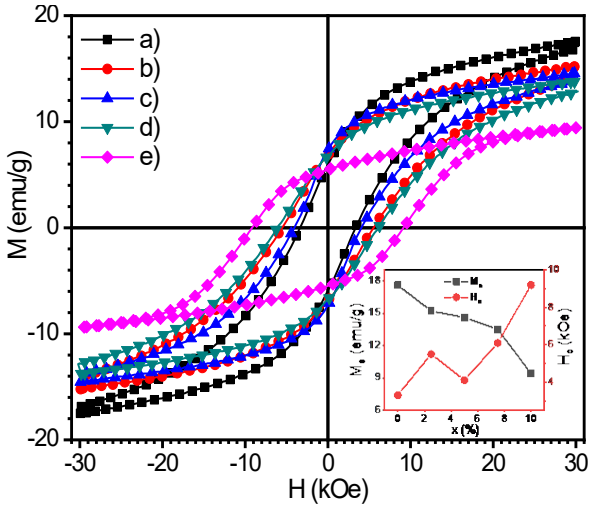

Figure 8. M(H) curves of $Mn_{55-x}Cr_xBi_{45}$ as spun ribbons: (a) x=0, (b) x = 2.5, (c) x= 5.0, (d) x = 7.5, and (e) x = 10.0.

In this sketch one observes the reduction of M_{sat} with the rate of about 0.8 emu·g^{-1}·x%$^{-1}$. This indicates a tendency for Cr atoms to substitute for manganese (Mn) at specific sites, which disrupts the long-range interactions between Mn atoms within the unit cell [34].

The non-smooth and uneven change of H_c versus x values is due to the fine nanocrystalline microstrucrue of ribbons that are illustrated on the FESEM images of the broken surfaces of $Mn_{55-x}Cr_xBi_{45}$ as-spun ribbon presented in Figure 9. The averaged grain sizes D are 54 nm, 75 nm, 50 nm, and 79 nm for as spun ribbons with x = 0 wt%, 2.5 wt%, 5.0 wt%, and 7.5 wt%, respectively. These values are much smaller than the single-domain size D_{sds} = 0.3 µm to 0.5 µm, causing H_c to be reduced by decreasing the grain size as described by the random anisotropy model for nanocrystalline material [35]. These microstructure graphs indicate that the changes in M_{sat} and H_c depend not only on the changes of interactions inside the unit cell but also on the microstructure of ribbons.

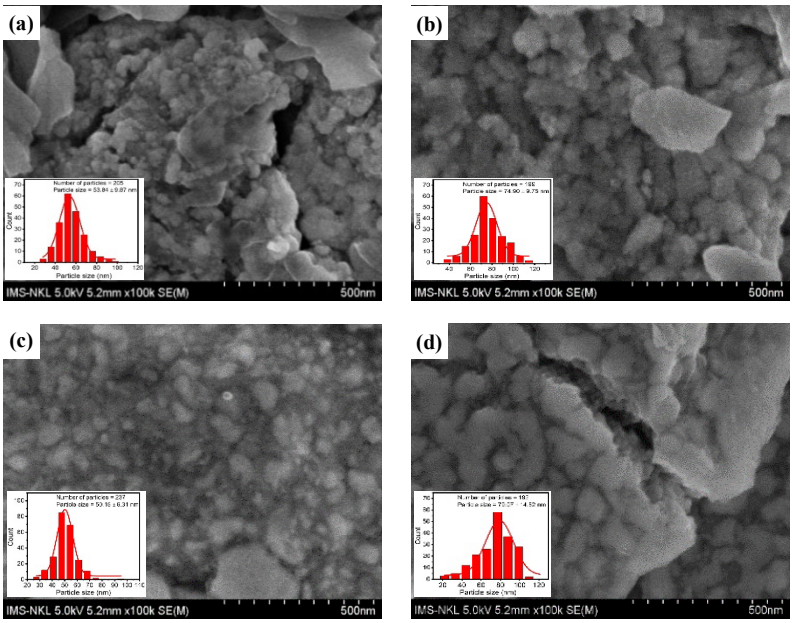

Figure 9. Field-emission scanning electron microscopy (FESEM) images of the fresh broken surfaces of $Mn_{55-x}Cr_xBi_{45}$ as spun ribbons: a) x=0, b) x = 2.5, c) x = 5.0, and d) x = 7.5. The cracks were appeared after the ribbons were broken.

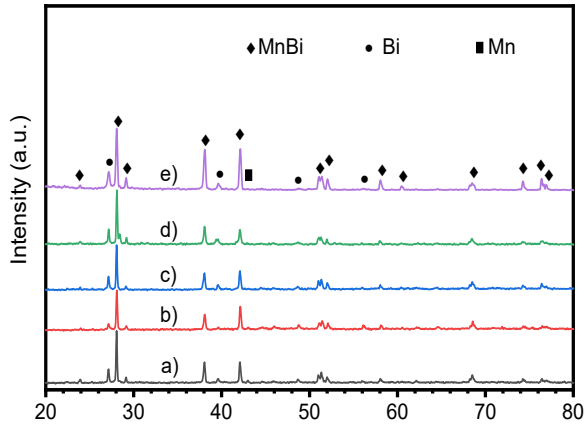

Figure 10. XRD patterns of $Mn_{55-x}Cr_xBi_{45}$ annealed ribbons: (a) x=0, (b) x = 2.5, (c) x= 5, (d) x = 7.5, and (e) x = 10.0.

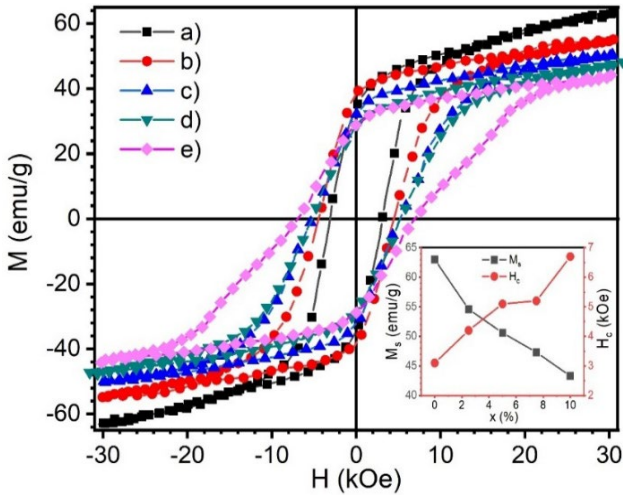

Figure 11. M(H) curves of $Mn_{55-x}Cr_xBi_{45}$ annealed ribbons: (a) x=0, (b) x = 2.5, (c) x= 5.0, (d) x = 7.5, and (e) x = 10.0.

It is understood that the ribbons quenched in the peritectic solidification leading to their low LTP content that is obligatory to use the prolonged anneal at the optimal annealing temperature of 300°C, at which the mutual Mn-Bi diffusion coefficient is high, to create MnBi phase without the appearance of high-temperature paramagnetic phase of $Mn_{1.08}Bi$. Figure 10 shows the phase evolution of prepared ribbons annealed at 300°C for 3 h. The LTP contents were increased and are 74 wt%, 65.8 wt%, 72.13 wt%, 70.65 wt%, and 72.94 wt% for the annealed ribbons with x = 0 wt%, 2.5 wt%, 5.0 wt%, 7.5 wt%, and 10.0 wt%, respectively. It is worthy to note that during the annealing there are no additional phase appeared.

The hysteresis loops of the annealed ribbons measured with the maximal measuring magnetic field of 30 kOe are shown in Figure 11, the M_{sat}, iH_c and $(BH)_{max}$ of these annealed ribbons are 63.0 emu·g^{-1}, 54.6 emu·g^{-1}, 50.6 emu·g^{-1}, 47.3 emu·g^{-1}, 43.3 emu·g^{-1}, 3.1 kOe, 4.2 kOe, 5.1 kOe, 5.2 kOe, 6.7 kOe and 2.86 MGOe, 3.64 MGOe, 2.59 MGOe, 2.04 MGOe, 2.11 MGOe for x = 0.0, 2.5, 5.0, 7.5, and 10.0, respectively.

In comparison with the literature data reported, our value of M_{sat} = 54.6 emu·g^{-1} for $Mn_{52.5}Cr_{2.5}Bi_{45}$ ribbon is comparable with the 54.2 emu·g^{-1} of M_{sat} reported in [22] for the ribbon $Mn_{47}Bi_{50}Cr_3$ melt-spun at the wheel speed of 19 m·s^{-1}. The sketch in Figure 11 illustrates the nearly linear changes by the slope of –1.7 emu·g^{-1}·x%$^{-1}$ for M_{sat} and +1.8 kOe·x%$^{-1}$ for H_c caused by varying x values of doped Cr.

One emphasizes the role of mutuality between the results of DFT calculation and the experimental ones in discussing the opportunity of Cr doping for improving the magnetic performance of MnBi melt-spun ribbons. First of all, it is worthy to note that the volume of unit cell is reduced by doping Cr atoms (see Table 1) with the rate of about 0.963 Å^3·x%$^{-1}$. This reduction of unit cell volume strengthens the interaction between atoms and is suggested to improve the magneto-crystalline anisotropy energy K_a and just the intrinsic coercivity as observed experimentally. Concerning the spontaneous magnetization M_{sp} one understood that this value can be increased or decreased depending on the complex interaction between all the atoms leading to the complex dependence of the ferromagnetism on the distance between atoms as observed on the Bethe-Slater curve [35]. Moreover, as discussed in [35] the ferromagnetic ground state arises as a consequence of the long-ranged interactions and the unit cell magnetization of MnBi is resulted from six terms of exchange interaction. All these evidences prove that the Cr doping can cause complicated change of M_{sp} that can be increased or decreased as discussed above in the section 3.1. More detail calculation shows that the M_{sp} of Cr-doped MnBi is decreased (see Table 2) and the experimental results support this tendency.

4. Conclusions

We systematically investigate the effects of chromium (Cr) doping on the intrinsic and extrinsic magnetic behaviors of MnBi-based alloys and melt-spun ribbons. Our findings combine the results of the first-principles density functional theory (DFT) calculations with the experimental characterizations. Theoretically, phonon dispersion simulations confirm that all Cr-doped MnBi structures exhibit no imaginary frequencies, indicating their dynamic stability. Formation energy calculations further demonstrate that Cr atoms preferentially substitute Mn rather than occupy interstitial sites, leading to modifications in the local magnetic environment. The DFT results indicate that the magnetic behavior in MnBi primarily originates from the Mn 3d orbitals. Including Cr can significantly alter the spin and orbital magnetic moments. Notably, all doped samples maintain their ferromagnetic nature but doping with a small amount of Cr (e.g., 5 at%) tends to enhance the overall magnetic moment, while a higher concentration of Cr (e.g., 10 at%) results in a slight decrease. On the experimental side, X-ray diffraction (XRD) patterns reveal the incorporation of Cr atoms into the lattice of MnBi, causing a slight effect on the interation within the unit cell, leading to a minor reduction in the Curie temperature T_c. Moreover, Cr doping has refined the grain size D and increased the coercivity field H_c. The predicted increase in spotaneoius magnetization M_{sp} from DFT calculation has not been observed in practice, limiting the magnetic energy product $(BH)_{max}$ and necessitating further research to improve the magnetic performance of Cr-doped MnBi in the near future.

Acknowledgment

We are grateful to acknowledge the financial support of the Vietnamese Ministry of Science and Technology (MOST) under the project NĐT/CN/21/25.

Declaration of interests

Truong Xuan Nguyen reports financial support was provided by Vietnamese Ministry of Science and Technology. If there are other authors, they declare that they have no known competing financial interests or personal relationships that could have appeared to influence the work reported in this paper.

References

[1] K. Ding, "The rare earth magnet industry and rare earth price in China," T*he European Physical Journal Conferences,* vol. 75, p. 04005, 2014.

[2] E. Adams, W. M. Hubbard, and A. M. Syeles, "A New permanent magnet from powdered manganese bismuthide, *Journal of Applied Physics*, vol. 23, pp. 1207-1211, 1952.

[3] J . Cui, J. P. Choi, G. Li, E. Polikarpov, J. Darsell, M. J. Kramer, N. A. Zarkevich, L. L. Wang, D. D. Johnson, M. Marinescu, Q. Z. Huang, H. Wu, N. V. Vuong, and J. P. Liu, "Development of MnBi permanent magnet: Neutron diffraction of MnBi powder, *Journal of Applied Physics*, vol. 115, p. 17A743, 2014.

[4] J. Park, Y. K. Hong, J. Lee, W. Lee, S. G. Kim, and C. J. Choi, "Electronic structure and maximum energy product of MnBi," *Metals (Basel)*, vol. 4, no. 3, pp. 455-464, 2014.

[5] M. Benaissa, "Theoretical investigation of structural, energetic and magnetic properties of B2 type MnM alloys, DFT and data mining approach," *Computational Condensed Matter*, vol. 31, p. e00656, 2022.

[6] K. Anand, J. J. Pulikkotil, and S.Auluck, "Effects of inter-site chemical disorder on the magnetic properties of MnBi," *Journal of Magnetism and Magnetic Materials,* vol. 363, pp. 18-20. 2014.

[7] V. Seshu Bai,vand T. Rajasekharan, "Evidence of a critical Mn-Mn distance for the onset of ferromagnetism in NiAs type compounds," *Journal of Magnetism and Magnetic Materials,* vol. 42, no. 2, pp. 198-200, 1984.

[8] P. Kharel, V. R. Shah, R. Skomski, J. E. Shield, D. J. Sellmyer, "Magnetism of MnBi-based nanomaterials," *IEEE Transactions on Magnetics*, vol. 49, no. 7, pp. 3318-3321, 2013.

[9] E. S. Olivetti, C. Curcio, L. Martino, M. Küpferling, and V. Basso, "Effect of Ti substitution on α and β phase formation and properties in $Mn_{50-x}Ti_xBi_{50}$ alloys," *Journal of Alloys and Compounds*, vol. 643, pp. S270-S274, 2015.

[10] S. Zhang, Z. Pengyue, H. C. Jiang, Y. Shi, N. Yu and H. Ge, "Magnetic and structural properties of MnBi1-xTixAlloys," *Journal of Magnetics*, vol. 19, no. 3, pp. 205-209, 2014.

[11] Y. Yang, J. W. Kim, P. Z. Si, H-D. Qian, Y. Shin, X. Wang, J. Park, O. L. Li, Q. Wu, H. Ge, and C-J. Choi, "Effects of Ga-doping on the microstructure and magnetic properties of MnBi alloys," *Journal of Alloys and Compounds*, vol. 769, pp. 813-816. 2018.

[12] P. Rani, A. Taya, and M. K. Kashyap, "Enhancement of magneto-crystalline anisotropy of MnBi with Co interstitial impurities," *AIP Conference Proceedings*, vol. 1942, no. 1, p. 130033, 2018.

[13] V. V. Ramakrishna, S. Kavita, R. Gautam, T. Ramesh, and R. Gopalan, "Investigation of structural and magnetic properties of Al and Cu doped MnBi alloy," *Journal of Magnetish and Magnetic Materials*, vol. 458, pp. 23-29, 2028.

[14] H. T. Nguyen, T. M. Man, and V. V. Nguyen, "Regulating the performance of MnBi magnetic materials by Sb doping: DFT calculations and experiments," *Journal of Electronic Materials*, vol. 49, no. 8, pp. 4962-4968, 2020.

[15] T. H. Nguyen, M. T. Man, H. M. Do, and V. V. Nguyen, "Magnetic properties and electronic structure of the Sb-doped MnBi from DFT calculations," *Solid State Communications*, vol. 336, p. 114385, 2021.

[16] P. Kainzbauer, K. W. Richter, H. S. Effenberger, G. Giester, and H. Ipser, "The ternary Bi-Mn-Sb phase diagram and the crystal structure of the ternary T phase $Bi_{0.8}MnSb_{0.2}$," *Journal of Phase Equilibria and Diffusion*, vol. 40, no. 4, pp. 462-481. 2019.

[17] A. M. Gabay, G. C. Hadjipanayis, and J. Cui, "Effect of Sb substitution on crystal structure, texture and hard magnetic properties of melt-spun MnBi alloys," *Journal of Alloys and Compounds*, vol. 792, pp. 77-86, 2019.

[18] N. Nereson, and G. Arnold, "Magnetic properties of CeBi, NdBi, TbBi, and DyBi," *Journal of Applied Physics*, vol. 42, no. 4, pp. 1625-1627, 1971.

[19] W. Y. Zhang, P. Khare, T. George, X. Z. Li, P. Mukherjee, S. Valloppilly, and D. J. Sellmyer, "Grain alignment due to magnetic-field annealing in MnBi:Bi nanocomposites," *Journal of Physics D: Applied Physics*, vol. 49, p. 455002, 2016.

[20] A. K. Vuong, N. X. Truong, L. Wei, H. V. Pham, N. H. Nguyen, N. H. Pham, Q. Nguyen, T. K. O. Vuong, V. H. Ky, X. Zhen, Y. Yang, and V. V. Nguyen, "Large-scale production and magnetic properties of Sn-substituted MnBi rare-earth-free melt-spun ribbons," *Applied Physics A*, vol. 130, no. 9, p. 630. 2024.

[21] https://environmentalchemistry.com/yogi/periodic/ionicradius.html.

[22] K. Anand, N. Christopher, and N. Singh, "Evaluation of structural and magnetic property of Cr-doped MnBi permanent magnet material," *Applied Physics A*, vol. 125, no. 12, p. 870, 2019.

[23] K. Anand, N. Christopher, and N. Singh, "Influence of wheel speed and ageing on nanostructure and magnetic properties of Cr-doped MnBi magnetic material," *Applied Physics A*, vol. 126, no. 5, p. 339, 2020.

[25] C. Chen, and S. P. Ong, "A universal graph deep learning inter-atomic potential for the periodic table," *Nature Computational Science*, vol. 2, no. 11, pp. 718-728, 2022.

[26] C. J. O. Verzijl, and J. M. Thijssen, "DFT-based molecular transport implementation in ADF/BAND," *Journal of Physical Chemistry C*, vol. 116, no. 46, pp. 24393-24412, 2012.

[27] L. Fan, and T. Ziegler, "Optimization of molecular structures by self-consistent and nonlocal density-functional theory," *Journal of Chemical Physics*, vol. 95, no. 10, pp. 7401-7408, 1991.

[28] J. P. Perdew, K. Burke, and M. Ernzerhof," Generalized gradient approximation made simple," *Physical Review Letters, vol.* 77, no. 18, pp. 3865-3868, 1996.

[29] M. Venkatraman, and J. P. Neumann, "The Bi−Cr (Bismuth-Chromium) system," *Bull Alloy Phase Diagrams,* vol. 9, no. 3, pp. 271-273, 1988.

[30] N. X. Truong, and N. V. Vuong, "Preparation and magnetic properties of MnBi alloy and its hybridization with NdFeB," *Journal of Magnetics*, vol. 20, no. 4, pp. 336-341, 2015.

[31] P. Kharel, B. Lama, M. Flesche, Z. Mehlberg, B. Lamsal, S. Valloppilly, Y. Zhou, D. Sellmyer, and T. Paudel, "Modifying magnetic properties of MnBi with carbon: An experimental and theoretical study," *Journal of Physics D: Applied Physics*, vol. 55, no. 26, p. 265003, 2022.

[32] K. Vero, and J. P. Borah, "Transformation of in-plane to out-of-plane anisotropy in MnBi alloy for permanent magnet application: A first-principles study," *Scientific Reports*, vol. 14, no. 1, p. 19015, 2024.

[33] J. Cui, J. P. Choi, E.i Polikarpov, M. E. Bowden, W. Xie, G. Li, Z. Nie , N. Zarkevich, M. J. Kramer, and D. Johnson, "Effect of composition and heat treatment on MnBi magnetic materials," *Acta Materialia*, vol. 79, pp. 374-381, 2014.

[34] M. E. McHenry, M. A. Willard, and D. E. Laughlin "Amorphous and nanocrystalline materials for applications as soft magnets," *Progress in Materials Science*, vol. 144, no. 4, pp. 291-433, 1999.

[35] G. Herzer, "Grain size dependence of coercivity and permeabilituy in nanocrystalline ferromagnets, *IEEE Transactions on magnetics*, vol. 26, pp. 1397-1402, 1990.